A single discrete Rab5-binding site in phosphoinositide 3-kinase β is required for tumor cell invasion

Samantha D. Heitz, David J. Hamelin, Reece M. Hoffmann, Nili Greenberg, Gilbert Salloum, Zahra Erami, … & Jonathan M. Backer

March 2019

A single discrete Rab5-binding site in phosphoinositide 3-kinase β is required for tumor cell invasion

Received for publication, September 28, 2018, and in revised form, January 15, 2019 Published, Papers in Press, January 18, 2019, DOI 10.1074/jbc.RA118.006032

Samantha D. Heitz[‡], David J. Hamelin[§], Reece M. Hoffmann[§], Nili Greenberg[‡], Gilbert Salloum[‡], Zahra Erami[‡], Bassem D. Khalil[‡1], Aliaksei Shymanets[¶2], Elizabeth A. Steidle[‡], Grace Q. Gong[‖3], Bernd Nürnberg[¶2], John E. Burke[§4], Jack U. Flanagan[‖3,5], Anne R. Bresnick[6], and Jonathan M. Backer[‡**7]**

From the Departments of [‡]Molecular Pharmacology and [**]Biochemistry, Albert Einstein College of Medicine, Bronx, New York 10461, [§]Department of Biochemistry and Microbiology, University of Victoria, Victoria V8P 3E6, British Columba, Canada, [¶]Department of Pharmacology and Experimental Therapy, Institute for Pharmacology and Toxicology and Interfaculty Center of Pharmacogenomics and Pharma Research, Eberhard-Karls-Universität Tübingen, Tübingen D-72074, Germany, and [‖]Molecular Medicine and Pathology, Maurice Wilkins Centre for Biodiscovery, The University of Auckland, Auckland Private Bag 92019, New Zealand

Edited by Henrik G. Dohlman

Phosphoinositide 3-kinase β (PI3Kβ) is regulated by receptor tyrosine kinases (RTKs), G protein–coupled receptors (GPCRs), and small GTPases such as Rac1 and Rab5. Our lab previously identified two residues (Gln^{596} and Ile^{597}) in the helical domain of the catalytic subunit (p110β) of PI3Kβ whose mutation disrupts binding to Rab5. To better define the Rab5–p110β interface, we performed alanine-scanning mutagenesis and analyzed Rab5 binding with an *in vitro* pulldown assay with GST-$Rab5^{GTP}$. Of the 35 p110β helical domain mutants assayed, 11 disrupted binding to Rab5 without affecting Rac1 binding, basal lipid kinase activity, or Gβγ-stimulated kinase activity. These mutants defined the Rab5-binding interface within p110β as consisting of two perpendicular α-helices in the helical domain that are adjacent to the initially identified Gln^{596} and Ile^{597} residues. Analysis of the Rab5–PI3Kβ interaction by hydrogen-deuterium exchange MS identified p110β peptides that overlap with these helices; no interactions were detected between Rab5 and other regions of p110β or p85α. Similarly, the binding of Rab5 to isolated p85α could not be detected, and mutations in the Ras-binding domain (RBD) of p110β had no effect on Rab5 binding. Whereas soluble Rab5 did not affect PI3Kβ activity *in vitro*, the interaction of these two proteins was critical for chemotaxis, invasion, and gelatin degradation by breast cancer cells. Our results define a single, discrete Rab5-binding site in the p110β helical domain, which may be useful for generating inhibitors to better define the physiological role of Rab5–PI3Kβ coupling *in vivo*.

Class I phosphoinositide 3-kinases (PI3Ks)[8] are lipid kinases that regulate cell motility, growth, and survival. Class IA PI3Ks are obligate heterodimers that contain a regulatory subunit (p85α/β, p55α/γ, or p50α) and a catalytic (p110α, -β, or -δ) subunit (1). The full-length regulatory p85 subunit consists of an N-terminal SH3 domain, two proline-rich domains (nPRD and cPRD) that flank a BCR homology domain (BCR), and two SH2 domains (N-terminal (nSH2) and C-terminal (cSH2)) linked by the inter-SH2 (iSH2) domain (1). The p110 catalytic subunit contains an N-terminal adaptor-binding domain (ABD), a Ras-binding domain (RBD), a C2 domain, a helical domain, and a C-terminal kinase domain (Fig. 1*A*) (2).

PI3Kβ can be activated by both receptor tyrosine kinase binding to the p85 SH2 domains (3) and by G protein–coupled receptors (GPCRs), which stimulate Gβγ binding to the C2–helical linker region of p110β (the Gβγ-binding loop) (Fig. 1*A*) (4, 5). In contrast to the other Class IA PI3Ks, which bind Ras, p110β binds the small GTPases Rac1 and Cdc42 via the RBD (6). Rab5 was first identified as a p110β-binding partner in a screen for Rab5 effectors (7). Rab5 localizes to early endosomes and other vesicular structures (8, 9), and PI3Kβ has been implicated in endocytic trafficking of cell-surface receptors (10, 11). Rab5 binding to p110β is required for macroautophagy induced by growth factor limitation (12).

This work was supported by National Institutes of Health Grants T32AG023475 (to S. D. H., Z. E., and E. A. S.), K12-GM102779 (to E. A. S.), R01 GM119279 (to J. M. B and A. R. B), and T32GM007491 (to N. G.) and the Macromolecular Therapeutics Core of the Albert Einstein Cancer Center through NCI, National Institutes of Health Grant CA013330. J. M. B. is on the scientific advisory board of Karus Therapeutics. The content is solely the responsibility of the authors and does not necessarily represent the official views of the National Institutes of Health.

This article contains Table S1.

[1] Present address: Laboratory of Signal Transduction, Memorial Sloan-Kettering Cancer Center, New York, NY 10065.

[2] Supported by Deutsche Forschungsgemeinschaft Grants GRK 1302 and NU 53/13-1.

[3] Supported by the Maurice Wilkins Centre for Biodiscovery.

[4] Supported by Cancer Research Society Operating Grant CRS-22641.

[5] Supported by Health Research Council of New Zealand Grant 13-763.

[6] To whom correspondence may be addressed. Tel.: 718-430-2741; E-mail: anne.bresnick@einstein.yu.edu.

[7] To whom correspondence may be addressed. Tel.: 718-430-2153; E-mail: jonathan.backer@einstein.yu.edu.

[8] The abbreviations used are: PI3K, phosphoinositide 3-kinase; GPCR, G protein–coupled receptor; RBD, Ras-binding domain; RBD-DM, RBD double mutant; SH, Src homology; PRD, proline-rich domain; iSH2, inter-SH2; nSH2, N-terminal nSH2; cSH2, C-terminal SH2; ABD, adaptor-binding domain; GTPγS, guanosine 5′-*O*-(thiotriphosphate); PIP_2, phosphatidylinositol 4,5-bisphosphate; KD, kinase-dead; HDX, hydrogen-deuterium exchange; PIP_3, phosphatidylinositol 3,4,5-trisphosphate; EGF, epidermal growth factor; LPA, lysophosphatidic acid; PMSF, phenylmethylsulfonyl fluoride; NP-40, Nonidet P-40; βME, β-mercaptoethanol; Ni-NTA, nickel-nitrilotriacetic acid; UPLC, ultraperformance LC; ANOVA, analysis of variance.

Our lab initially identified a region of p110β that mediates binding to Rab5 using a conservation-based approach. Two residues were identified (Q596C and I597S) whose mutation disrupts binding to Rab5 (13). The purpose of the present study was to fully define the Rab5-binding interface within p110β to understand the physiological role of this interaction. Using a GST-Rab5 *in vitro* pulldown assay and hydrogen-deuterium exchange MS, we identified a discrete binding site for Rab5 in the helical domain of p110β. We were unable to replicate previous reports showing direct binding of Rab5 to p85 or to the RBD of p110β (14, 15). The Rab5-binding interface within p110β is restricted to two perpendicular α-helices in the helical domain that are located near the Gβγ-binding loop. *In vitro* kinase assays revealed that soluble Rab5 does not affect PI3Kβ kinase activity. However, replacement of endogenous PI3Kβ with a Rab5 binding– deficient mutant in MDA-MB-231 breast cancer cells inhibited chemotaxis, invasion, and gelatin degradation. Our characterization of the physiologically important Rab5–p110β interface will facilitate the development of better tools to study the Rab5–PI3Kβ interaction in cell-based and animal models.

Results

Rab5 binds exclusively to the helical domain of p110β

To define the Rab5-binding interface within p110β (PI3Kβ), we first examined whether p110β selectively bound to any of the three Rab5 isoforms (A, B, and C), which have been shown to have distinct cellular roles (8, 16, 17). Using lysates from HEK293T cells expressing wild type (WT) PI3Kβ heterodimer and an *in vitro* pulldown assay, we were unable to detect any difference in PI3Kβ binding to the three Rab5 isoforms (data not shown). We opted to use Rab5A for the remainder of the study as this isoform was previously used by our lab and by others in studies examining the Rab5–p110β interaction (13, 15).

HEK293T cells were transfected with p85α alone or with either WT p110β or the previously reported Rab5-uncoupled p110β mutant I597S (13). The lysates from these cells were incubated with nucleotide-loaded Rab5A beads and assessed for binding by immunoblotting. The WT p110β/p85α heterodimer exhibited selective binding to GTPγS–Rab5A (12-fold over GDP–Rab5), whereas the Rab5-uncoupled p110β I597S heterodimer failed to bind to either form of Rab5A (Fig. 1*B*). In contrast to previous reports that Rab5 binds to p85α (14), we did not detect binding of Rab5A to p85α alone (Fig. 1*B*). Similarly, we detected no binding to p85α in the context of the I597S p110β/p85α heterodimer. These data show that p110β is solely responsible for the Rab5A interaction.

We previously identified two residues in the helical domain of p110β (Gln^{596} and Ile^{597}) whose mutation disrupts binding to GST-Rab5 (13). To more completely map the Rab5–p110β interface, we mutated additional residues in the helical domain of p110β and evaluated the effect on binding to Rab5A. We chose 35 surface-accessible residues surrounding Gln^{596}/Ile^{597}. Lysates from transfected cells expressing p85α and WT or mutant p110β were incubated with nucleotide-loaded GST-Rab5A beads and assessed for binding via immunoblotting (Fig. 1*C*). For each mutant, we calculated the percentage of the input (lysate) that bound to GTPγS–Rab5A; values in each experiment were normalized to WT p110β binding, which was set to 100%.

The relative binding of the p110β mutants to WT p110β was stratified into three groups: 0–33% binding (*red*), 33–66% binding (*blue*), and >66% binding (*green*). Of the 35 mutated helical domain residues tested, eight showed binding that was less than 33% of WT, and four showed binding that was 33–66% of WT (Figs. 1*D* and 2). Residues whose mutation significantly inhibited Rab5 binding mapped to two α-helices (Asp^{509}–Glu^{517} and Leu^{585}–Ile^{597}), which are located below the Gβγ-binding loop (Fig. 1*E*). The mutagenesis data suggest the primary Rab5 interface localizes to a discrete region within the helical domain of p110β.

The RBD of p110β does not bind Rab5A

A previous study reported that the RBD mediates Rab5 binding to p110β (15). However, this study evaluated Rab5 binding using a nonphysiological, truncated iSH2 domain–p110β fusion rather than full-length p85α/p110β. To reexamine the role of the p110β RBD in Rab5 binding in the context of the full-length heterodimer, we mutated the five amino acids in the RBD that were previously assessed for Rab5 binding (15). Using the GST-Rab5A pulldown assay and lysates from cells expressing p85α and p110β (Fig. 3*A*), all five p110β RBD mutants exhibited binding to Rab5A that was comparable with WT p85α/p110β (Fig. 3, *B* and *C*). These data indicate that residues in the p110β RBD are not involved in Rab5 binding.

Mutations in p110β that disrupt Rab5 binding do not affect binding to Rac1

To ensure that the mutations affecting p110β binding to Rab5A did not compromise the overall structure or folding of the p110β subunit, we examined the binding of p110β mutants to another small GTPase, Rac1, which binds to the p110β RBD (6). Previous studies demonstrated that mutation of two residues in the RBD (S211D and K230A) was sufficient to disrupt binding to GTPγS–Rac1 (6). We compared the binding of p85α/p110β heterodimers to GST-Rac1 and GST-Rab5 in our *in vitro* pulldown assay (Fig. 4*A*). Binding of WT p110β to GTPγS–Rab5 was 3.3-fold higher than to GTPγS–Rac1 (17.7% of input as compared with 5.4% of input) (Fig. 4*B*). This is consistent with Fritsch *et al.* (6), who observed *in vitro* that p110β exhibited weaker binding to Rac1 than to Rab5. Also consistent with previous studies (18, 19), we could detect binding of p85α to GST-Rac1 (data not shown). However, binding was weak compared with p110β (1% of the input, even when using 4-fold more p85α lysate as compared with p85α/p110β heterodimer lysates). Thus, the binding of Rab5 and Rac1 to p85α is negligible as compared with their binding to p110β.

As expected, the I597S mutant did not bind active Rab5A but did bind to active Rac1. Conversely and consistent with the observations of Fritsch *et al.* (6), the RBD-DM mutant of p110β bound active Rab5A but not Rac1 (Fig. 4*C*). Using the *in vitro* pulldown assay with GTPγS-loaded GST-Rac1, we also tested the newly identified Rab5-uncoupled p110β mutants as heterodimers with p85α. All of the helical domain mutants tested exhibited binding to GST-Rac1 that was comparable with that seen with WT p110β (Fig. 4, *D* and *E*). In addition, mutations in

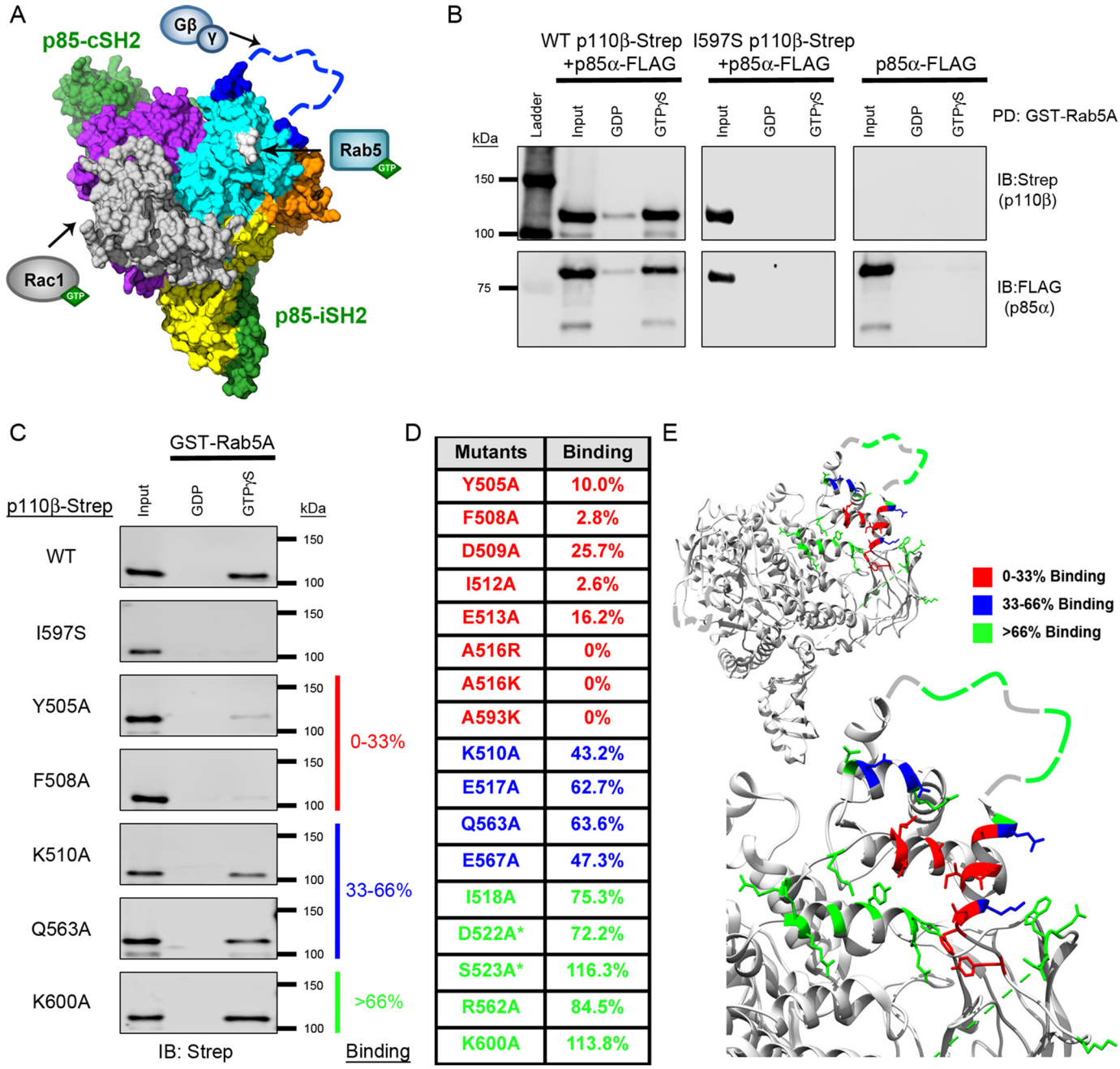

Mutants	Binding
Y505A	10.0%
F508A	2.8%
D509A	25.7%
I512A	2.6%
E513A	16.2%
A516R	0%
A516K	0%
A593K	0%
K510A	43.2%
E517A	62.7%
Q563A	63.6%
E567A	47.3%
I518A	75.3%
D522A*	72.2%
S523A*	116.3%
R562A	84.5%
K600A	113.8%

Figure 1. Mutagenesis of the p110β helical domain disrupts Rab5A binding to PI3Kβ. *A*, space-filling model of the murine p110β catalytic subunit with the iSH2 and cSH2 domains of the p85β regulatory subunit (*green*) (Protein Data Bank (PDB) code 2Y3A). *Yellow*, the N-terminal ABD; *gray*, the RBD; *orange*, the C2 domain; *cyan*, the helical domain; *purple*, the C-terminal kinase domain. The *blue dashed line* represents the C2–helical linker, which was not observed in the X-ray structure. The *arrows* indicate where Rac1, Rab5, and Gβγ bind to p110β. Gln^{596}/Ile^{597}, whose mutation disrupts Rab5 binding, are shown in *white*. *B*, representative immunoblots (*IB*) of the GST-Rab5A pulldown (*PD*) assay. Human GST-Rab5A was immobilized on GSH-agarose beads and loaded with GDP or GTPγS. The beads were incubated with whole-cell lysates (*Input*) from HEK293T cells transfected with p85α-FLAG without or with WT p110β-Strep or the Rab5-uncoupled I597S mutant. *C*, representative immunoblots of the GST-Rab5A pulldown assay with p110β mutants. Samples were analyzed by SDS-PAGE and blotted for Strep (p110β) and FLAG (p85α). *D*, table of Rab5A-binding activity for representative p110β mutants. Binding to GTPγS–Rab5A was calculated as a percentage of the input and then normalized to WT p110β binding, which was set to 100%. Binding, as compared with WT p110β, was stratified into three groups: 0–33% (*red*), 33–66% (*blue*), and >66% (*green*). Residues in the Gβγ-binding loop are indicated with an *asterisk*. *E*, ribbon diagrams of p110β (*upper panel*) and a magnified view of the helical domain (*lower panel*). Residues are color-coded based on their Rab5A-binding activity (PBD code 2Y3A).

the RBD that were reported to disrupt Rab5 binding (15) showed no significant difference in binding to GST-Rac1 with the exception of I234A, which is near the previously identified RBD-DM mutations (S211D and K230A) (Fig. 4, *E* and *F*). These data demonstrate that p110β mutations that disrupt Rab5 binding do not affect the binding of Rac1 to p110β.

p110β mutations that disrupt Rab5 binding do not affect PI3Kβ kinase activity or activation by Gβγ

To verify that the enzymatic activity of the p110β helical domain mutants was intact, we performed *in vitro* kinase assays. For these assays, we selected a subset of p110β mutants: F508A and I512A, which showed <33% binding to GTP-loaded

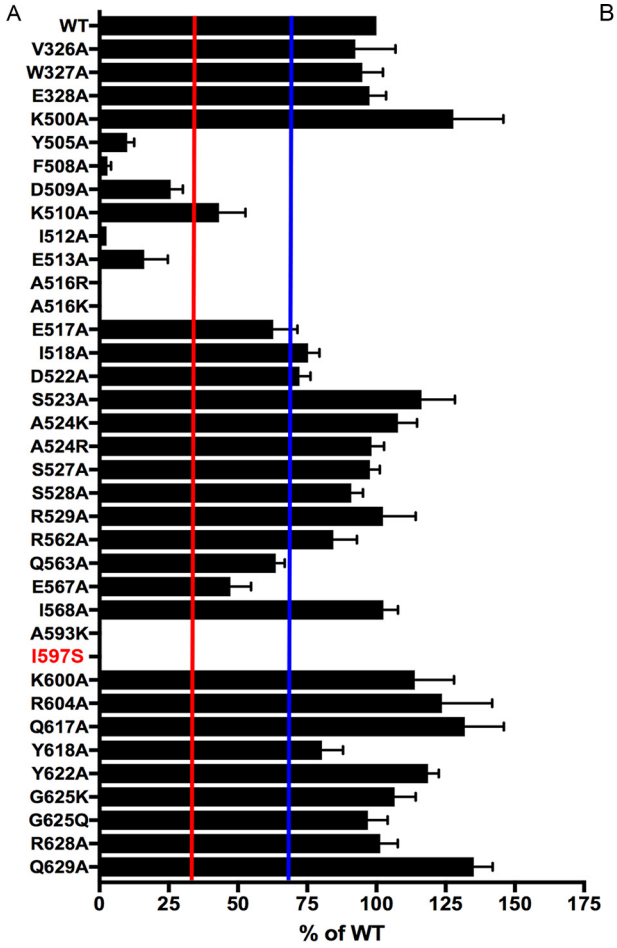

B

Mutants	Binding	P-value
V326A	92.45%	0.9991
W327A	94.9%	0.9994
E328A	97.5%	0.9997
K500A	127.8%	0.2664
Y505A	10%	0.0001
F508A	2.8%	0.0001
D509A	25.7%	0.0001
K510A	43.2%	0.0002
I512A	2.6%	0.0001
E513A	16.2%	0.0001
A516R	0%	0.0001
A516K	0%	0.0001
E517A	62.7%	0.0411
I518A	75.3%	0.4297
D522A*	72.2%	0.2679
S523A*	116.3%	0.9303
A524K*	107.8%	0.9991
A524R*	98.2%	0.9998
S527A*	97.7%	0.9997
S528A*	91.0%	0.9988
R529A*	102.4%	0.9997
R562A	84.5%	0.9563
Q563A	63.6%	0.0501
E567A	47.3%	0.0006
I568A	102.5%	0.9997
A593K	0%	0.0001
I597S	0%	0.0001
K600A	113.8%	0.9844
R604A	123.7%	0.4900
Q617A	132.0%	0.1269
Y618A	80.3%	0.7563
Y622A	118.6%	0.8215
G625K	106.6%	0.9993
G625Q	97.0%	0.9997
R628A	101.4%	0.9999
Q629A	135.2%	0.1392

Figure 2. Helical domain mutations in p110β exhibit variable binding to GST-Rab5A. *A*, quantification of the Rab5A-binding activity for all p110β mutants as compared with WT. Data represent the mean ± S.E. from three independent experiments. *Error bars* represent S.E. The *red* and *blue lines* indicate 33 and 66% binding, respectively. *B*, table showing the average Rab5A-binding activity for all p110β mutants relative to WT p110β. *Red*, 0–33%; *blue*, 33–66%. Statistical analyses were performed using one-way ANOVA. Residues in the Gβγ-binding loop are indicated with an *asterisk*.

Rab5 relative to WT, and K510A and E517A, which showed 33–66% binding relative to WT (Fig. 5*A*). The p85α/p110β heterodimers were expressed in HEK293T cells, isolated on Strep-Tactin beads, and eluted with desthiobiotin. The eluted product was then assayed for activity using vesicles containing 2.9 mol % phosphatidylinositol 4,5-bisphosphate (PIP_2) as a substrate. As expected, the negative control kinase-dead (KD; K805R) p110β exhibited minimal kinase activity. The Rab5-uncoupled mutants of p110β exhibited specific activities comparable with WT p110β (Fig. 5*B*). These data demonstrate that the basal kinase activity of p110β is unaffected by mutations in the helical domain.

To determine whether the p110β mutants responded to a known activator of p110β, we measured *in vitro* kinase activity in the presence of purified Gβγ (5). We chose Gβγ because the Gβγ-binding loop is in close proximity to the Rab5-binding interface in the p110β helical domain. Heterodimers of p85α with WT or mutant p110β showed an ~2-fold activation by Gβγ (p values <0.01; Fig. 5, *C* and *D*); the I512A mutant, which showed a 2-fold activation, trended toward significance (p = 0.0712). In contrast, a mutation known to disrupt Gβγ binding to PI3Kβ (K532D/K533D (5)) abolished activation by Gβγ (Fig. 5*E*). Taken together, our data show that helical domain mutations that disrupt Rab5 binding have no effect on the other biochemical activities of p110β.

Hydrogen-deuterium exchange MS (HDX-MS) analysis of the Rab5-binding site in p110β

To examine the Rab5-binding site in p110β by an orthogonal approach, we used HDX-MS. Experiments were carried out at five time points (3 s at 1 °C as well as 3, 30, 300, and 3000 s at 18 °C). Sequence coverages of 86.8 and 90.2% were achieved for p110β and p85α with 155 and 104 peptides, respectively. Decreases in hydrogen-deuterium exchange rates (>5%) were observed within the helical domain of p110β in peptides spanning residues His^{492}–Glu^{513} and Arg^{566}–Leu^{578} (Fig. 6, *A* and *C*). Peptide His^{492}–Glu^{513} (Fig. 6*A*, *right panel*) overlaps with α-helix Asp^{509}–Glu^{517}, which was critical for Rab5 binding in the pulldown assay (Fig. 6*A*, *left panel*). Peptides corresponding to the other critical α-helix, Leu^{585}–Ile^{597}, were not detected in the MS analysis. However, the Arg^{566}–Leu^{578} peptide (Fig. 6*A*, *right panel*) includes Glu^{567} whose mutation caused a greater than 50% decrease in Rab5 binding (Fig. 6*A*, *left panel*). An increase in the rate of hydrogen-deuterium exchange was also observed in the kinase domain of p110β in peptides spanning residues Asn^{729}–Met^{742} (Fig. 6, *B* and *C*). No significant

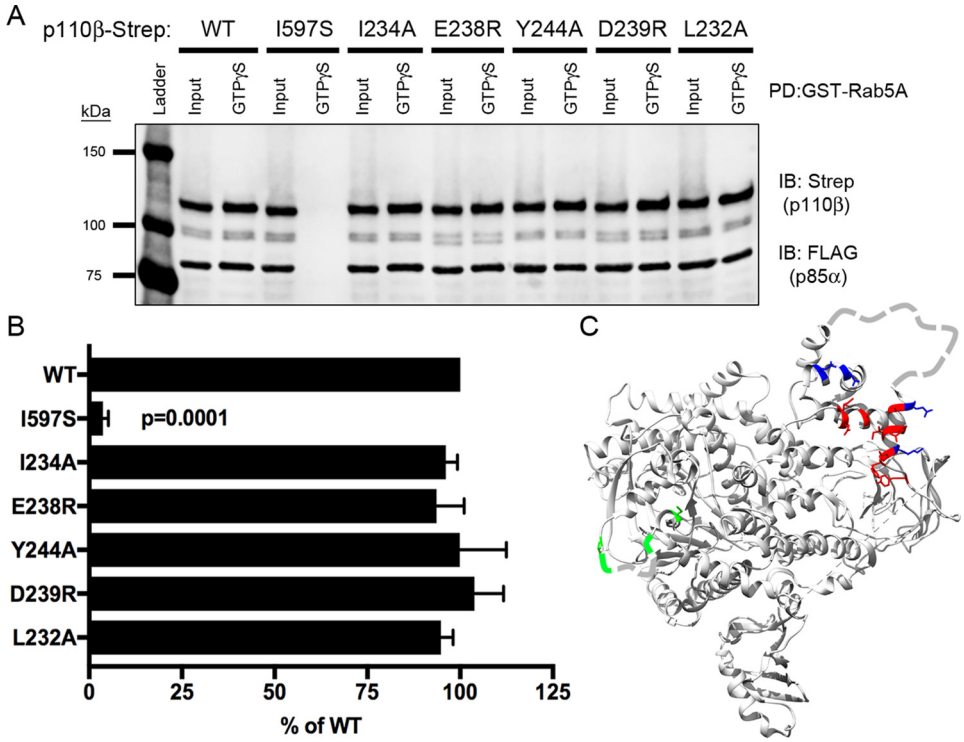

Figure 3. Mutation of the p110β RBD does not affect binding to Rab5. *A*, representative immunoblot (*IB*) of GST-Rab5A pulldown (*PD*) assay showing lysates from cells expressing select RBD p110β mutations incubated with GST-Rab5A beads and blotted for Strep and FLAG. *B*, quantification of Rab5A binding. The data represent the mean ± S.E. from three independent experiments. *Error bars* represent S.E. Statistical analyses were performed using one-way ANOVA. No statistical differences were observed between WT and RBD p110β mutant proteins. *C*, ribbon diagram of p110β showing residues in the helical domain and RBD that were targeted for mutagenesis. Color coding reflects Rab5-binding activity relative to WT p110β: *red*, 0–33%; *blue*: 33–66%; *green*, >66%. Residues in the RBD and Gβγ-binding loop that are not observed in the X-ray structure are depicted as *dashed lines*.

changes were observed in the RBD of p110β or in the p85α regulatory subunit. The HDX-MS data support our findings that regions Tyr^{505}–Glu^{517} and Ala^{589}–Ile^{597} of the helical domain of p110β constitute the single Rab5-binding interface.

Soluble $Rab5^{GTP}$ does not stimulate PI3Kβ kinase activity in vitro

We performed lipid kinase assays with recombinant PI3Kβ and GDP- or GTP-loaded Rab5 using lipid vesicles containing 2.9 mol % PIP_2 as a substrate. Although the addition of 1 μM tyrosyl phosphopeptide caused a 26-fold activation of PI3Kβ (from 0.054 to 1.43 pmol of PIP_3/min), addition of 10 μM Rab5 had minimal effect on PI3Kβ kinase activity (0.01 and 0.02 pmol/min for GDP- and GTP-loaded Rab5, respectively) (Fig. 7*A*). Binding of GTP-loaded Rab5 to PI3Kβ was confirmed by pulldown with immobilized p85α/p110β heterodimer bound to Strep-Tactin beads (Fig. 7*B*).

Rab5–PI3Kβ interactions are required for tumor cell chemotaxis, invasion, and gelatin degradation

Previous work from our lab established a role for GPCR-mediated PI3Kβ kinase activity in breast cancer metastasis (20). To study the role of Rab5 binding to PI3Kβ in metastasis-associated cellular activities, we used stable knockdown/rescue MDA-MB-231 cells that express the murine myc-tagged WT and Rab5-uncoupled p110β mutant (I591S) at similar levels (Fig. 8*A*). In a transwell migration assay, chemotaxis toward LPA was reduced by ~70% in cells expressing the Rab5-uncoupled mutant (Fig. 8*B*); chemotaxis toward EGF was reduced by ~50% (Fig. 8*C*). Similar results were observed with a transwell invasion assay in which EGF-stimulated invasion through Matrigel was reduced by ~50% in cells expressing Rab5-uncoupled PI3Kβ (Fig. 8*D*).

Metastasis requires that tumor cells invade from the primary tumor into the surrounding extracellular matrix. To investigate the role of the Rab5–PI3Kβ interaction in matrix degradation, we compared the matrix-degrading activity of MDA-MB-231 knockdown/rescue cells expressing murine WT, KD (K799R) or Rab5-uncoupled mutant p110β. Cells were plated on fluorescently labeled gelatin, and the area of degradation per cell was measured (Fig. 8, *E* and *F*). Expression of either p110β mutant inhibited gelatin degradation by 80–90%. Taken together, these data suggest a critical role for Rab5 binding to PI3Kβ in the motility and invasion of breast tumor cells.

Discussion

We previously described a p110α/p110β chimera, which contained the N terminus of p110α (ABD and RBD) linked to the C terminus of p110β (C2, helical, and kinase domains) (21) and showed that it could bind to GST-Rab5 (13). Subsequent mutagenesis studies identified two residues (Gln^{596} and Ile^{597}) in the helical domain whose mutation to the corresponding residues in p110δ abolished binding to Rab5 (13). The present study used two independent techniques, structure-directed alanine-scanning mutagenesis and HDX-MS, to unambiguously define the full Rab5-binding interface within the catalytic subunit (p110β) of PI3Kβ.

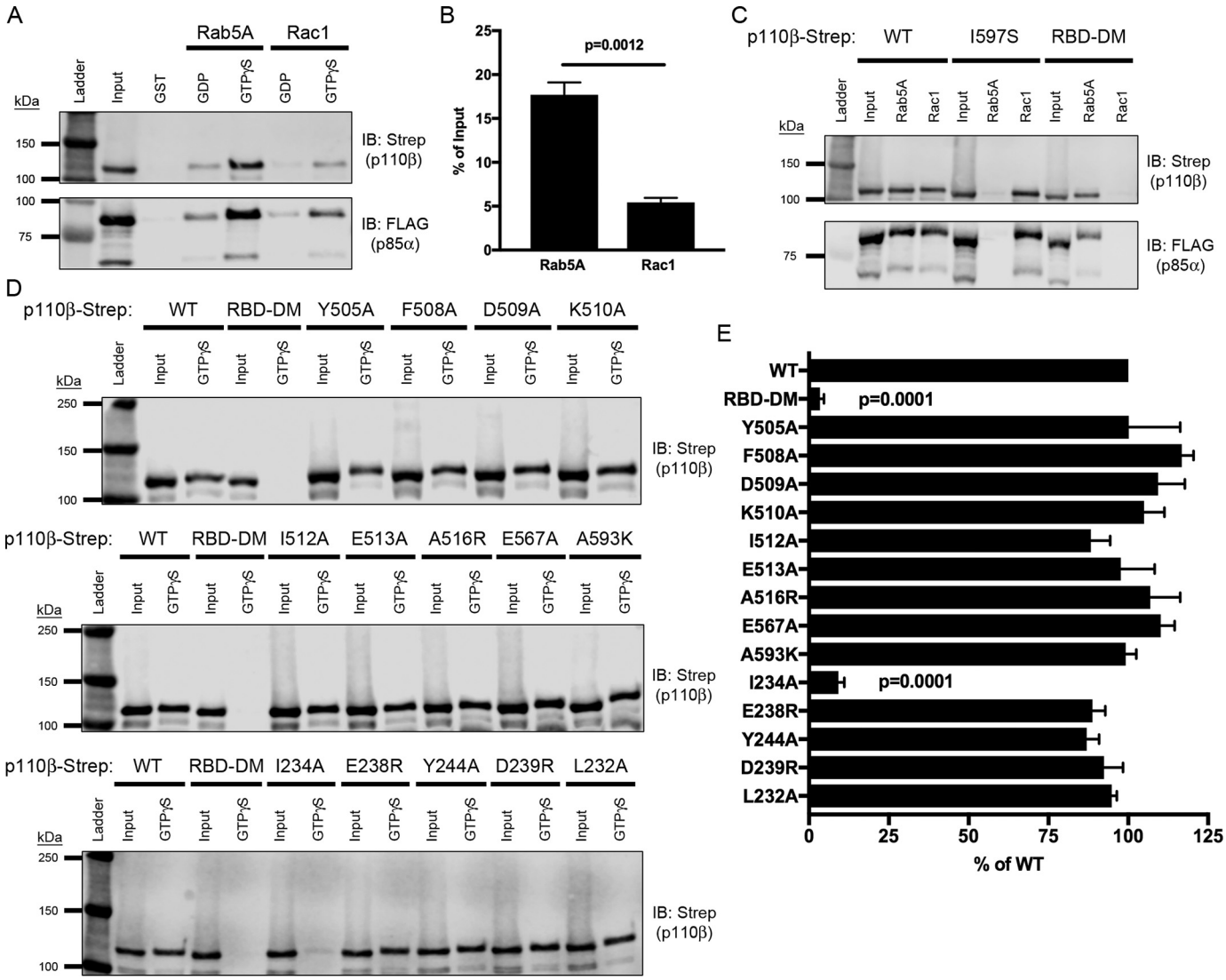

Figure 4. Mutation of the Rab5-binding interface does not disrupt binding to Rac1. *A*, representative immunoblot (*IB*) of GST-Rab5A and GST-Rac1 pulldown assay. Lysates expressing WT p110*β*-Strep/p85*α*-FLAG were incubated with GST-Rab5A and GST-Rac1 beads loaded with nucleotide and assessed for binding via SDS-PAGE and immunoblotting for Strep and FLAG. *B*, quantification of PI3K*β* binding to GTPγS–Rac1 or Rab5A, expressed as a percentage of the input. Data represent the mean ± S.E. from three independent experiments. Statistical analysis was performed using an unpaired Student's *t* test. *C*, representative immunoblot of GTPγS-loaded GST-Rab5A and GST-Rac1 pulldowns incubated with lysates expressing p85*α*-FLAG and WT, I597S, or Rac1-uncoupled mutant (RBD-DM) p110*β*-Strep. *D*, GST-Rac1 binding assay with lysates expressing Rab5-uncoupled helical domain and RBD p110*β* mutants analyzed by SDS-PAGE and immunoblotted with Strep. *E*, quantification of the percent binding as compared with WT p110*β*. Data represent the mean ± S.E. from three independent experiments. *Error bars* represent S.E. in all panels. Statistical analyses were performed using one-way ANOVA. No statistically significant difference was observed, unless indicated.

Our screen identified specific residues in the helical domain of p110*β* (Tyr^{505}, Phe^{508}, Asp^{509}, Ile^{512}, Glu^{513}, Ala^{516}, and Ala^{593}) that are critical for Rab5A binding (mutation leads to <33% of WT binding). These residues are located within two perpendicular *α*-helices (Asp^{509}–Glu^{517} and Leu^{585}–Ile^{597}; human sequence) that are situated just below the G*βγ*-binding loop (Fig. 1*A*) (3). Residues critical for Rab5 binding in helices Asp^{509}–Glu^{517} and Leu^{585}–Ile^{597} have their side chains oriented toward a common surface (Fig. 1*E*). We believe that these residues make up the main Rab5-binding interface. In contrast, residues Lys^{510} and Glu^{517} have side chains that are oriented away from the primary Rab5-binding interface, and their mutation caused only a partial reduction in binding (33–66%). Two residues whose mutation showed limited effects on Rab5 binding (Gln^{563} and Glu^{567}) are found on a helix that is parallel to and above helix Leu^{585}–Ile^{597}; these residues most likely define the distal edge of the Rab5-binding interface. Our mutagenesis studies define a discrete binding site, as residues critical for binding were surrounded by residues whose mutation did not affect the interaction.

HDX-MS experiments identified two peptides, His^{492}–Glu^{513} and Arg^{566}–Leu^{578}, which were protected from solvent exchange by p110*β* binding to GTP–Rab5. His^{492}–Glu^{513} overlaps significantly with the Asp^{509}–Glu^{517} helix identified in our screen. Arg^{566}–Leu^{578} includes a residue (Glu^{567}) whose mutation decreases binding by over 50%. Although a decrease in solvent accessibility in these peptides could be due to a secondary conformational change caused by Rab5 binding, their coincidence with the region identified by our mutagenesis studies suggests that the changes are due to direct Rab5 binding. Inter-

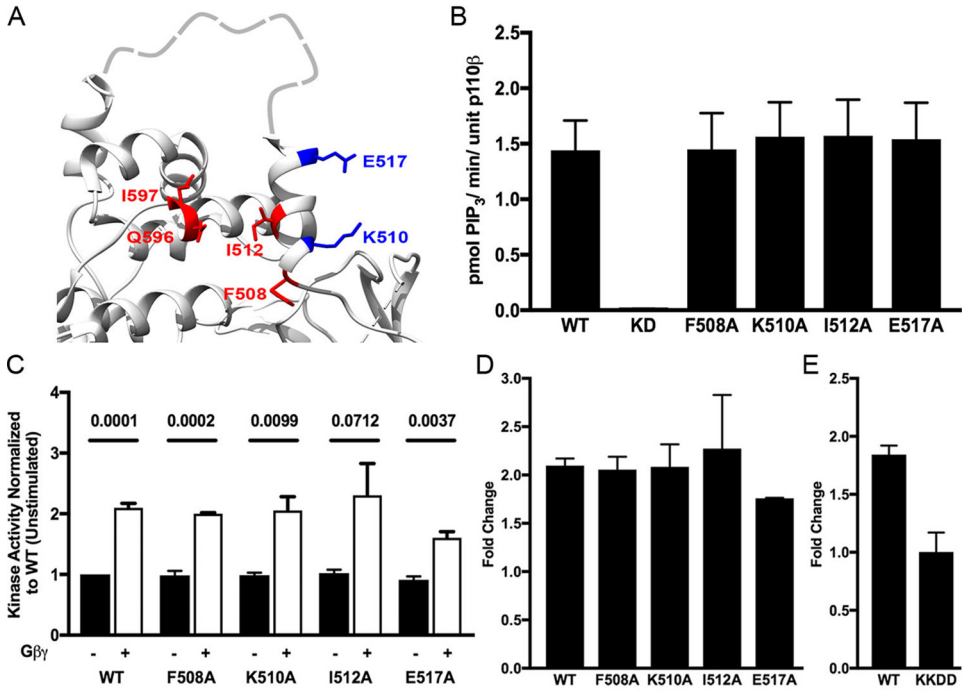

Figure 5. Mutation of the Rab5-binding interface does not affect PI3Kβ kinase activity or activation by G$\beta\gamma$. *A*, ribbon diagram of the p110β helical domain showing the original Rab5-uncoupled mutations (Gln^{596}/Ile^{597}) and mutated residues selected for *in vitro* kinase assays. Color coding corresponds to relative Rab5-binding activity: residues Phe^{508} and Ile^{512} (*red*), 0–33%; Lys^{510} and Glu^{517} (*blue*), 33–66%. *B*, quantification of *in vitro* kinase activity for WT p110β, KD (K805R) p110β, and the four helical domain p110β mutants. Values were normalized to the amount of p110β in each reaction as determined by immunoblotting. Data represent the mean ± S.E. for four independent experiments. Statistical analyses were performed using one-way ANOVA. Significance was observed for the difference in kinase activity between WT and KD ($p = 0.0097$), but no significant difference was observed between WT and other mutants of p110β. *C*, quantification of *in vitro* kinase activity without (*black bars*) and with (*white bars*) G$\beta\gamma$, normalized to unstimulated WT p110β activity. Data represent the mean ± S.E. for three independent experiments. Statistical analyses were performed using an unpaired Student's *t* test. *D*, quantification of the -fold change in kinase activity with G$\beta\gamma$ stimulation. Data represent the mean ± S.E. for three independent experiments. Statistical analyses were performed using one-way ANOVA. There was no significant difference in the -fold activation for WT and mutant p110β. *E*, activation of WT and G$\beta\gamma$-uncoupled (K532D/K533D (*KKDD*)) PI3Kβ by G$\beta\gamma$ was determined as in *D*. The data are the mean ± S.D. from two experiments. *Error bars* represent S.E. in panels *B*, *C* and *D*, and S.D. in panel *E*.

estingly, Asn^{729}–Met^{742} from the kinase domain showed an increase in solvent exposure upon incubation with Rab5A, presumably due to a secondary conformational change. This region of p110β has been reported to interact with membranes (5), suggesting that conformational changes in p110β upon Rab5 binding could promote membrane targeting and provide a possible mechanism of activation, similar to that observed with the p110α oncogenic H1047R mutation (22).

We verified that mutation of the helical domain did not affect the overall functionality of p110β by measuring binding to Rac1. For WT p110β, we observed 3-fold greater binding to Rab5 as compared with Rac1, but mutation of the Rab5-binding site had no effect on Rac1 binding, and mutation of the RBD did not affect Rab5 binding. Similarly, mutations that disrupt Rab5 binding did not affect basal PI3Kβ activity or its activation by G$\beta\gamma$. Given the proximity of the Rab5- and G$\beta\gamma$-binding sites in p110β, activation by G$\beta\gamma$ is an important control for the specificity of mutations that disrupt Rab5 binding. We did observe a modest reduction in the activation of the E517A mutant by G$\beta\gamma$, perhaps because this residue resides at the base of the G$\beta\gamma$-binding loop (5). Importantly, our biochemical analyses demonstrate that the loss of Rab5 binding in the mutants described here is not due to overall, nonspecific disruptions or indirect conformational changes of the p110β structure.

Of note, previous reports about the effect of Rab5 binding on p110β kinase activity are conflicting. In *in vitro* kinase assays performed with nonlipidated Rab5, we could not detect any effect on p110β kinase activity. Further studies with prenylated or membrane-targeted Rab5 will be required to fully explore the regulation of PI3Kβ kinase activity by Rab5.

Metastasis is a complex process that involves the migration and invasion of tumor cells though the extracellular matrix, intravasation into blood vessels, and extravasation at distal sites (23). Both invasion and transendothelial migration require the formation of degradative structures called invadopodia, actin-rich protrusions that promote the secretion of matrix metalloproteases (20). Work from our lab previously showed that G$\beta\gamma$ coupling to p110β activity in breast cancer cells is critical for macrophage-induced invasion, matrix degradation, and tumor extravasation (20). We now show that the PI3Kβ–Rab5 interaction is similarly necessary for EGF-mediated chemotaxis and invasion as well as gelatin degradation. Currently, we do not understand how PI3Kβ binding to Rab5 regulates these processes. However, Rab5 is required for matrix degradation, through its regulation of endocytic trafficking and activation of Rac1 (24). Given that Rac1 and PI3Kβ can form a positive feedback loop in some cell types (25), it is possible that PI3Kβ–Rab5 interactions may contribute to the endosomal activation of Rac1.

Our data are not in agreement with earlier studies on the PI3K–Rab5 interaction by the Anderson and co-workers (14), who reported that the p85α regulatory subunit binds to Rab5 in a nucleotide-independent manner. We could not detect bind-

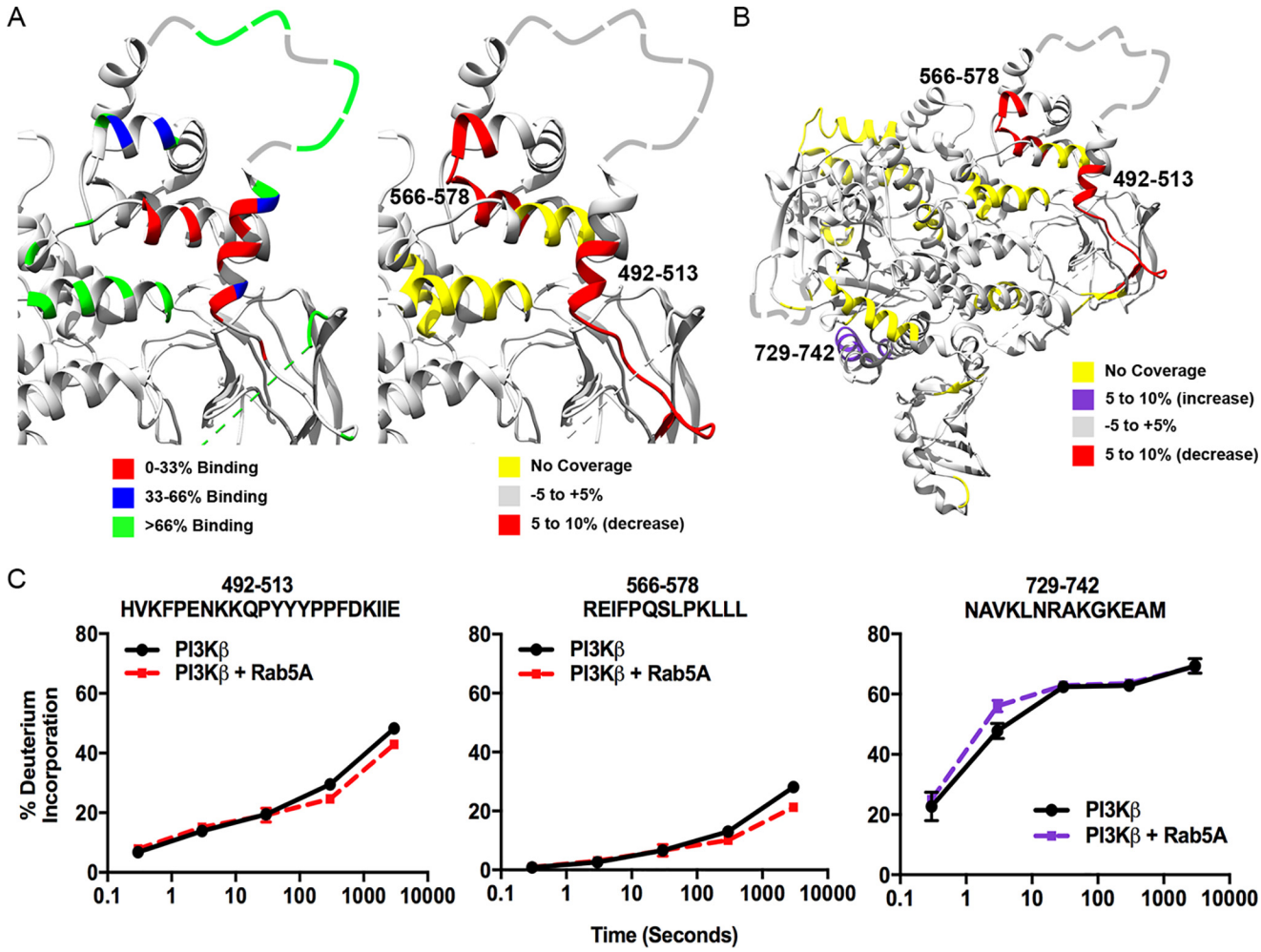

Figure 6. HDX-MS revealed changes within the helical domain of p110β upon interaction with soluble Rab5A. HDX-MS experiments were carried out for PI3Kβ in the absence or presence of a 7.5-fold molar excess of soluble Rab5A. *A*, *left panel*, representation of the p110β helical domain with Rab5-uncoupled mutants color-coded by relative Rab5 binding as compared with WT. *Right panel*, representation of the p110β helical domain showing peptides that exhibited changes in deuteration in the presence of Rab5A. *B*, representation of the full-length p110β showing all peptides that exhibited significant changes in deuteration in the presence of Rab5A (>5% and 0.5-Da difference in deuterium incorporation and *p* value of <0.01 based on a Student's *t* test). *C*, time course of deuterium incorporation for select peptides in the absence (*solid black line*) or presence (*dashed line*) of Rab5A. Data represent the mean ± S.E. for three independent experiments. For most data points the *error bars*, which represent S.E., are contained within the *symbols*.

ing of Rab5 to p85α alone or to p85α when expressed as a heterodimer with the Rab5-uncoupled mutant, I597S p110β. Our data are consistent with the original study that identified p110β as a Rab5-interacting protein (7) and that demonstrated Rab5 binding to *in vitro* translated p85α/p110β heterodimer and to the p110β catalytic subunit, but not to p85α.

Whitecross and Anderson (15) recently reported that the RBD of p110β binds Rab5. However, this study used a chimera in which a fragment of the p85α iSH2 domain was linked to the N terminus of p110β via a short seven-residue glycine linker (15). The truncated iSH2 (residues 466–567) has not been biochemically or structurally characterized. Furthermore, the truncated iSH2 domain deletes residues that mediate interactions with the C2 domain of p110α (27) and p110β (3) and whose deletion or mutation leads to oncogenic activation of PI3Kα (29–31). Thus, the chimera is unlikely to accurately reflect the conformation of the full-length p85α/p110β heterodimer. Importantly, our study, which used full-length p85α and p110β, demonstrated that the p110β mutants described by Whitecross and Anderson (15) exhibit WT levels of binding to Rab5. Consistent with these findings, HDX-MS analysis failed to detect interactions between Rab5 and either p85 or the RBD of p110β, despite being present in 7.5-fold molar excess.

In summary, we have defined a single, discrete binding site for Rab5 in PI3Kβ, comprising two perpendicular α-helices in the helical domain. Individual point mutants in this region abolish PI3Kβ–Rab5 binding, but have no effect on PI3Kβ binding to Rac1 or PI3Kβ kinase activity, under basal or Gβγ-stimulated conditions. Using both biochemical and biophysical approaches, we could not detect any contributions from the RBD of p110β or from the p85α regulatory subunit to Rab5 binding. Mutation of the Rab5-binding site in PI3Kβ in breast cancer cells has significant inhibitory effects on tumor cell motility and invasion and blocks matrix degradation. The unambiguous determination of a single Rab5-binding site will facilitate the development of biochemical tools to further study the functions of this interaction in tumor metastasis and other physiological and pathophysiological cell behaviors.

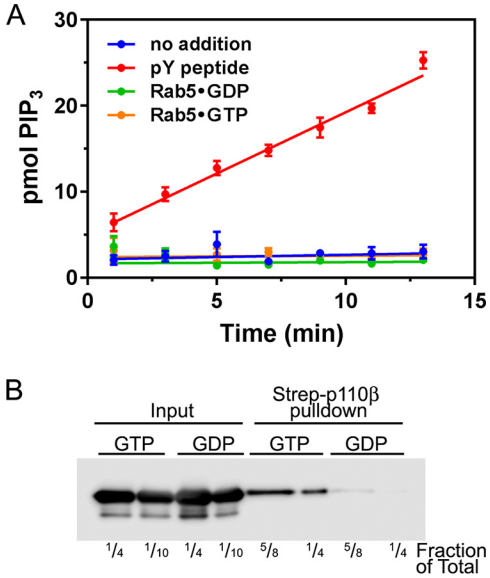

Figure 7. Rab5^{GTP} does not affect PI3Kβ kinase activity *in vitro*. Purified recombinant PI3Kβ was incubated with 10 μM Rab5, which had been loaded with GDP or GTPγS, or 1 μM tyrosine bisphosphopeptide (*pY peptide*). *A*, lipid kinase activity toward lipid vesicles (2.9 mol % PIP_2) was determined as described. The data are the mean ± S.E. from three independent experiments. *Error bars* represent S.E. *B*, p85-FLAG/p110β-StrepII was produced in HEK293T cells and immobilized on Strep-Tactin beads. The beads were incubated with GDP- or GTP-loaded Rab5, washed, and then analyzed by SDS-PAGE and Western blotting with Rab5 antibodies. The lanes show $^1/_4$ or $^1/_{10}$ of the input and $^5/_8$ or $^1/_4$ of the pulldowns.

Experimental procedures

Plasmids and mutagenesis

Full-length WT human Rab5A, Rab5B, and Rab5C (kindly provided by Dr. Philip Stahl, Washington University) were subcloned into the BamHI and XhoI sites of the bacterial expression vector pGEX-6P1 (GE Healthcare). WT Rac1 was cloned into pGEX-6P1 using the AgeI and EcoRI sites. WT human p85α-FLAG(×3) (kindly provided by Dr. Roger Williams, Cambridge) was subcloned into the pcDNA3.3 vector. WT human p110β (original construct provided by Dr. Roger Williams, Cambridge) was subcloned into a linearized pcDNA3.3-StrepII(×3) vector by In-Fusion HD cloning (Takara Bio). The linearized pcDNA3.3-StrepII(×3) vector was generated by digestion with XhoI and BamHI. The Rab5-uncoupled p110β (I597S) mutant was produced by QuikChange site-directed mutagenesis (Agilent). Additional p110β mutants were created by synthesizing fragments of p110β and subcloning into the p110β-StrepII(×3) construct: Lys^{499}–Glu^{662} for helical domain mutants, Val^{209}–Ile^{269} for the Rac1-uncoupled mutant (S211D/K230A; RBD-DM), and Phe^{148}–Leu^{591} for the other p110β RBD mutants (L232A, I234A, E238R, D239R, and Y244A).

Protein expression and purification for binding assays

BL21-Gold(DE3) cells (Agilent) were transformed with human GST-Rab5A, -B, or -C in pGEX-6P1. Bacteria were grown at 37 °C for 18 h in autoinduction medium (1.33% (w/v) tryptone, 2.67% (w/v) yeast extract, 1.0% (v/v) glycerol, 25 mM $(NH_4)_2SO_4$, 50 mM KH_2PO_4, 50 mM Na_2HPO_4, 2.5% (w/v) glucose, 10% (w/v) α-lactose, 1 mM $MgSO_4$) (32). The bacteria were collected by centrifugation at 8000 × *g* for 10 min at 4 °C and then resuspended in Rab5 lysis buffer (50 mM Tris-HCl, pH 8.0, 100 mM NaCl, 2 mM EDTA, 10% (v/v) glycerol, 1% (w/v) CHAPS, 2 mM DTT, Pierce protease inhibitor tablet (Thermo Fisher), 2 mM PMSF). The cells were sonicated in an ice bath with a microprobe tip (Branson) at 40% amplitude for four cycles of 20 s on, 40 s off. Triton X-100 was added to the cell suspension to a final concentration of 1% (v/v). The lysate was rotated for 20 min at 4 °C and centrifuged at 27,000 × *g* for 30 min at 4 °C. The supernatant was applied to a column of GSH-agarose beads (Thermo Fisher) twice. The column was washed with 20 column volumes of wash buffer (50 mM Tris-HCl, pH 8.0, 100 mM NaCl, 2 mM EDTA, 10% (v/v) glycerol, 1% (w/v) CHAPS, 2 mM DTT). GST-Rab5 was eluted from the beads with 20 column volumes of wash buffer containing 15 mM reduced L-GSH (Sigma-Aldrich) and dialyzed for 8 h against nucleotide loading buffer (25 mM Tris-HCl, pH 7.5, 50 mM NaCl, 10 mM EDTA, 5 mM $MgCl_2$, 0.06% (w/v) CHAPS, 2 mM DTT) with three buffer changes.

Human WT GST-Rac1 was expressed in bacteria as described above. The pellets were resuspended in Rac1 lysis buffer (50 mM Tris-HCl, pH 7.6, 50 mM NaCl, 5 mM $MgCl_2$, 1 mM DTT, Pierce protease inhibitor tablet, 2 mM PMSF). The lysates were clarified, and GST-Rac1 was purified as described above using wash buffer (50 mM Tris-HCl, pH 7.6, 50 mM NaCl, 5 mM $MgCl_2$, 1 mM DTT) and elution buffer (50 mM Tris-HCl, pH 7.6, 150 mM NaCl, 1 mM DTT, 25 mM reduced L-GSH (Sigma-Aldrich)). Purification of lipidated $G\beta_1\gamma_2$ protein was performed as described previously (33).

p85α and p110β expression in HEK cells

HEK293T cells (ATCC) were cultured in Dulbecco's modified Eagle's medium containing 10% fetal bovine serum at 37 °C with 5% CO_2. Cells were transfected with human p85α-FLAG(×3) alone or with human p110β-StrepII(×3) constructs using polyethylenimine (Polysciences) (34). The transfected cells were grown for 48 h, trypsinized, washed, and aliquoted into three equal fractions per 10-cm plate. Cells were pelleted at 830 × *g* for 5 min at 4 °C, frozen in liquid nitrogen, and stored at −80 °C.

Frozen transfected cell pellets were resuspended in pulldown lysis buffer (20 mM Tris-HCl, pH 7.4, 150 mM NaCl, 20 mM $MgCl_2$, 10% (v/v) glycerol, 0.06% (w/v) CHAPS, 0.1% (v/v) NP-40, 1 mM DTT, Pierce protease inhibitor tablet, 2 mM PMSF), rotated for 20 min at 4 °C, and centrifuged at 17,900 × *g* for 5 min at 4 °C. Total protein concentrations were determined using the Bio-Rad DC Protein Assay.

GST-Rab5/GST-Rac1 binding assays

GSH-agarose beads were incubated with 1.0 nmol of GST, GST-Rab5A, or GST-Rac1 protein overnight at 4 °C. The beads were washed three times with nucleotide loading buffer and loaded with either 1 mM GDP (Sigma) or GTPγS (Sigma) for 15 min at 30 °C in loading buffer. $MgCl_2$ was added to the beads to a final concentration of 20 mM. The beads were incubated at 30 °C for 3 min and then transferred to ice for 20 min. After nucleotide loading, the beads were washed with nucleotide stabilization buffer (25 mM Tris-HCl, pH 7.5, 50 mM NaCl, 20 mM $MgCl_2$, 0.06% (w/v) CHAPS, 2 mM DTT) containing 10 μM nucleotide, GDP, or GTPγS.

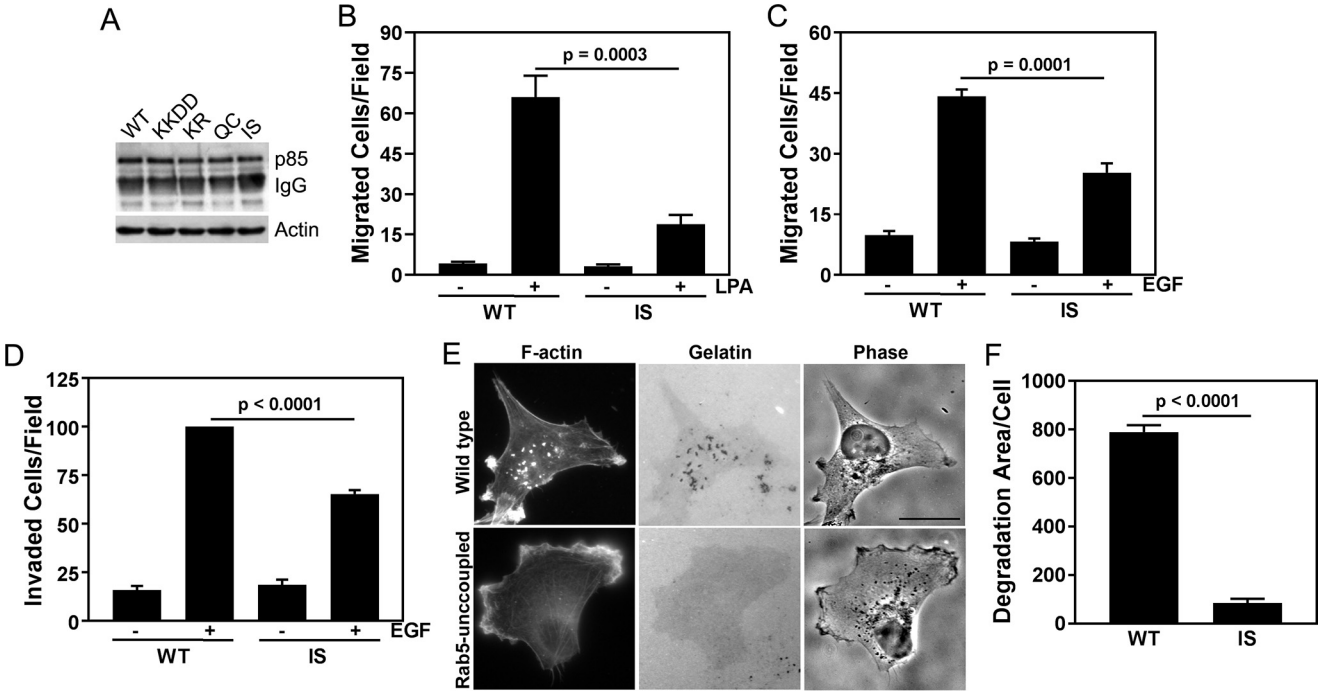

Figure 8. Rab5 binding to p110β is required for chemotaxis, invasion, and gelatin degradation by breast cancer cells. *A*, myc immunoprecipitation and p85 blotting of p110β knockdown MDA-MB-231 cells stably expressing murine WT, Gβγ-uncoupled (K526D/K527D (*KKDD*)), kinase-dead (K799R (*KR*)), or Rab5-uncoupled p110β (Q590C (*QC*) or I591S (*IS*)). *B*, LPA-stimulated (10 μM) chemotaxis of MDA-MB-231 p110β knockdown cells stably expressing murine WT p110β or the Rab5-uncoupled p110β mutant (*IS*). Data represent the mean ± S.E. from three independent experiments. *C*, EGF-stimulated (5 nM) chemotaxis of MDA-MB-231 p110β knockdown cells stably expressing murine WT p110β or the Rab5-uncoupled p110β mutant (I591S). Data represent the mean ± S.E. from three independent experiments. *D*, transwell Matrigel invasion assay toward 5 nM EGF of MDA-MB-231 p110β knockdown cells stably expressing WT or I591S p110β. The data were normalized to the number of invaded cells expressing WT p110β and represent the mean ± S.E. for three independent experiments. *E*, MDA-MB-231 cells expressing WT or I591S p110β were plated on Oregon Green 488–conjugated gelatin for 18 h, fixed, and stained with rhodamine phalloidin. *Scale bar* = 20 μm. *F*, degradation area per cell for MDA-MB-231 p110β knockdown cells stably expressing WT or I591S p110β. *Error bars* represent S.E. in all panels. Statistical analyses were performed using one-way ANOVA (*B*, *C*, and *D*) or Student's *t* test (*E*).

HEK293T cell lysates (100 μg of total protein) were incubated with the GST beads in the presence of 10 μM nucleotide (either GDP or GTPγS) for 1 h on a rotating wheel at 4 °C. The beads were washed four times with nucleotide stabilization buffer and 10 μM nucleotide and boiled in 2× Laemmli sample buffer.

One-third of the eluted bead samples and 1/20 of the input samples (5 μg of total protein) were separated by 7.5% SDS-PAGE and analyzed by immunoblotting. Membranes were incubated with a rabbit StrepII antibody (Abcam, ab76949) and a mouse FLAG antibody (Sigma, F4042) in Odyssey Blocking Buffer (LI-COR Biosciences). Goat anti-rabbit (LI-COR Biosciences, 925-68071) and goat anti-mouse (LI-COR Biosciences, 925-32210) antibodies conjugated to IR dyes were used with a LI-COR Biosciences Odyssey Fc Imaging System and Image Studio Lite software to visualize and quantify the bands.

The input values were multiplied by 20 to determine the total p110β incubated with the beads. The sample values for GST-Rab5 binding and GST-Rac1 binding were corrected to account for the fraction of the eluted samples that was loaded on the gel. The percentage of input bound was calculated by dividing the total sample values (bead-bound p110β) by the total input values and multiplying by 100. To pool data from individual experiments, binding was normalized to Rab5-GTP or Rac1-GTP binding for WT PI3Kβ in each experiment

Lipid kinase assay

Human p85α-FLAG(×3) and human p110β-StrepII(×3) were transiently coexpressed in HEK293T cells. Cell pellets were lysed in lysis buffer (50 mM Tris-HCl, pH 7.4, 150 mM NaCl, 1 mM $CaCl_2$, 1 mM $MgCl_2$, 10% (v/v) glycerol, 1% (v/v) NP-40, Pierce protease inhibitor tablet, 2 mM PMSF, 1 mM DTT, phosphatase inhibitor mixtures 2 and 3 (Sigma)) as described above. Strep-Tactin Superflow agarose beads (EMD Millipore) were washed once with lysis buffer and then incubated with 1600 μg of total cell lysate for 1.5 h while rotating at 4 °C. The beads were washed three times with PBS, pH 7.4, 1% (v/v) NP-40; three times with 100 mM Tris-HCl, pH 7.4, 500 mM LiCl; once with 10 mM Tris-HCl, pH 7.4, 100 mM NaCl, 1 mM EDTA; and once with kinase assay buffer (20 mM PIPES, pH 6.5, 100 mM NaCl, 0.05% (w/v) CHAPS, 1 mM DTT). The p85α/p110β heterodimer was eluted from the beads with kinase assay buffer containing 2.5 mM D-desthiobiotin (EMD Millipore).

Lipid vesicles were prepared in 250-μl batches by combining 153 nmol of 1-palmitoyl-2-oleoyl-*sn*-glycero-3-phospho-L-serine, 242 nmol of 1-palmitoyl-2-oleoyl-*sn*-glycero-3-phosphocholine, 14.8 nmol of PIP_2, and 98 nmol of cholesterol (Avanti Polar Lipids). The lipids were dried down under nitrogen gas, lyophilized overnight, resuspended in 250 μl of reaction buffer plus 2 mM EGTA, and sonicated with a cup horn for 10 min (Fisher Scientific, 550 Sonic Dismembrator).

Lipid vesicles (37 μl) were incubated on ice for 30 min with 1.5 μM purified $G\beta_1\gamma_2$ protein or an equal volume of $G\beta_1\gamma_2$ buffer (33). The eluted p110β-StrepII(×3)/p85α-FLAG(×3) heterodimer (9 μl) was incubated with the lipid vesicles with or

without $G\beta_1\gamma_2$ for 10 min at room temperature. The reaction volume was brought to 55 μl with kinase assay buffer. To start the reaction, 5 μl of the ATP mixture (100 μM ATP containing 10 μCi of [^{32}P]ATP final) was added and incubated for 10 min at room temperature before spotting duplicate 4-μl samples on nitrocellulose (35). Once dry, the nitrocellulose was washed twice with wash buffer (1 M phosphoric acid, 1 M NaCl) for 1 min and then four more times for 5 min. Total counts in each reaction mixture were determined by spotting diluted samples (1:20) onto nitrocellulose without washing. Radioactivity was quantitated using a PhosphorImager (GE Healthcare).

The relative units of p110β in each reaction were calculated by loading equal volumes of the p110β elutions for 7.5% SDS-PAGE and immunoblotting as described above. To normalize the intensity values across experiments, a standard curve of purified KD p110β-StrepII(×3) was included on each blot. The slope (intensity/μl) of the best-fit line for the standards was used to calculate the relative units of the p110β sample by dividing the intensity of the sample by the slope. This was then corrected to represent the total units of p110β in the reaction.

Protein expression and purification for HDX-MS

BL21(DE3) cells were transformed with constitutively active Rab5A Q79L (Agilent). Bacterial cultures in 2× YT (Sigma) broth (16 g/liter tryptone, 10 g/liter yeast extract, 5 g/liter NaCl) were induced with 0.5 mM isopropyl 1-thio-β-D-galactopyranose after growth to an A_{600} of 0.6–0.8 and then grown at 37 °C for an additional 4 h. The bacteria were harvested by centrifugation, washed with ice-cold PBS, and resuspended in lysis buffer (20 mM Tris-HCl, pH 7.5, 100 mM NaCl, 2 mM βME, protease inhibitor mixture set III (Sigma)). The cells were sonicated on ice for 5 min (10 s on, 10 s off, level 6.0; Misonix Sonicator 3000). Triton X-100 was added to the lysate to a final concentration of 0.1% (v/v) and centrifuged at 20,000 × *g* for 45 min.

The supernatant was loaded at a flow rate of 2 ml/min onto two 5-ml GSTrap HP columns (GE Healthcare) in tandem, pre-equilibrated with 30 ml of H_2O followed by 30 ml of Hep A buffer (20 mM Tris-HCl, pH 7.5, 100 mM NaCl, 2 mM βME). The columns were washed with 50 ml of Hep A buffer, and the GST tag was cleaved by incubating the column with 10 ml of lipoyl domain-Tev protease solution containing 10 mM βME on ice overnight. The protein was eluted with 20 ml of Hep A. Imidazole was added to a final concentration of 10 mM.

The cleaved Rab5A was loaded onto a 5-ml HisTrap FF column (GE Healthcare) pre-equilibrated with 10 ml Ni-NTA buffer A (20 mM Tris-HCl, pH 7.5, 100 mM NaCl, 10 mM imidazole, pH 8.0, 2 mM βME) to remove the His-tagged lipoyl domain-Tev. The flow-through and a 10-ml Ni-NTA buffer A wash were pooled and concentrated to 1 ml using a 10,000 molecular weight cutoff Amicon concentrator (Millipore). GTPγS was added in a 2-fold molar excess relative to Rab5A along with 25 mM EDTA. After incubation for 1 h at room temperature, the solution was exchanged with gel filtration buffer (20 mM HEPES, pH 7.0, 150 mM NaCl, 1 mM $MgCl_2$) and concentrated to a final volume of 900 μl. $MgCl_2$ was added to 30 mM, and the solution was incubated for 10 min on ice. Rab5A was purified using a Superdex 75 10/300 GL size exclusion column (GE Healthcare) equilibrated in gel filtration buffer.

To express PI3Kβ, an optimized ratio of p110β:p85α baculovirus was used to coinfect 1–2 × 10^6 cells/ml *Spodoptera frugiperda* (Sf9) cells. Coinfections were harvested after 40–72 h and washed with ice-cold PBS before flash freezing in liquid nitrogen. Frozen Sf9 cells were resuspended in lysis buffer (20 mM Tris-HCl, pH 8.0, 20 mM imidazole, pH 8.0, 100 mM NaCl, 5% (v/v) glycerol, 2 mM βME, protease inhibitor mixture set III) and sonicated on ice for 1.5 min (15 s on, 10 s off, level 4.0; Misonix Sonicator 3000). Triton X-100 was added to the lysate to a concentration of 0.2% (v/v) and centrifuged at 20,000 × *g* for 45 min. The supernatant was loaded onto two 5-ml HisTrap FF columns in tandem, equilibrated in Ni-NTA buffer A (20 mM Tris-HCl, pH 8.0, 100 mM NaCl, 20 mM imidazole, pH 8.0, 5% (v/v) glycerol, 2 mM βME). The columns were washed with 20 ml of high-salt wash buffer (20 mM Tris-HCl, pH 8.0, 1000 mM NaCl, 20 mM imidazole, pH 8.0, 5% (v/v) glycerol, 2 mM βME) and 20 ml of Ni-NTA buffer A followed by 20 ml of 6% Ni-NTA buffer B (20 mM Tris-HCl, pH 8.0, 100 mM NaCl, 300 mM imidazole, pH 8.0, 5% (v/v) glycerol, 2 mM βME) before being eluted with Ni-NTA buffer B.

The eluate was loaded onto two 1-ml StrepTrap HP columns (GE Healthcare) equilibrated in Hep A buffer (20 mM Tris-HCl, pH 8.0, 100 mM NaCl, 5% (v/v) glycerol, 2 mM βME). To cleave the streptavidin tag, the proteins were loaded with a solution of LipTev protease in 10 mM βME and incubated at 4 °C overnight. The protein was eluted by passing Hep A buffer through the columns. The StrepTrap elution was concentrated using a 50,000 molecular weight cutoff Amicon concentrator (Millipore). The concentrated protein was additionally purified using a Superdex 200 Increase 10/300 GL size exclusion column (GE Healthcare) equilibrated with gel filtration buffer (20 mM HEPES, pH 7.5, 150 mM NaCl, 0.5 mM tris(2-carboxyethyl)phosphine).

HDX-MS

HDX experiments were carried out as described previously (28). In brief, experiments were performed in a 5-μl reaction volume with final PI3Kβ and Rab5A concentrations of 1.6 and 12 μM, respectively. The two conditions tested consisted of PI3Kβ incubated with or without Rab5A for a duration of 10 min. Deuterium exchange was initiated by the addition of 3.35 μl of D_2O buffer (10 mM HEPES, pH 7.5, 100 mM NaCl, 99% (v/v) deuterium oxide). Exchange was evaluated at five time points (3 s at 1 °C as well as 3, 30, 300 and 3000 s at 18 °C) and was terminated by the addition of 65 μl of quench buffer (2 M guanidine HCl, 3% formic acid). All experiments were carried out in triplicate. Samples were immediately frozen in liquid nitrogen and stored at −80 °C.

Samples were quickly thawed and injected onto an ultraperformance LC (UPLC) system at 2 °C. Samples were loaded onto two immobilized pepsin columns (Applied Biosystems, Poroszyme) at 10 and 2 °C, respectively, at a flow rate of 200 μl/min for 3 min. Peptides were collected and desalted on a VanGuard precolumn trap (Waters) and loaded onto an ACQUITY 1.7-μm particle, 100 × 1 mm C_{18} UPLC column (Waters). Separation and elution of peptides from the analytical column were achieved using a gradient of 5–36% mobile phase B (Buffer A, 0.1% formic acid, LC/MS grade; Buffer B, 100% acetonitrile,

LC/MS grade) over 16 min. Mass spectrometry experiments were performed using an Impact II TOF (Bruker) with acquisition over a mass range of 150 to 2200 m/z using an electrospray ionization source operated at 200 °C and a spray voltage of 4.5 kV. Peptides were identified using a data-dependent acquisition approach following MS/MS experiments (0.5-s precursor scan from 150 to 2000 m/z; 12 0.25-s fragment scans from 150 to 2000 m/z). MS/MS data sets were analyzed using PEAKS7 (PEAKS), and the false discovery rate was set at 1% using a database of purified proteins and known contaminants.

HD-Examiner software (Sierra Analytics) was used to automatically calculate the level of deuterium incorporation into each peptide. All peptides were manually inspected for correct charge state and the presence of overlapping peptides. Deuteration levels were calculated using the centroid of the experimental isotope clusters. The results for these proteins are presented as relative levels of deuterium incorporation, and the only control for back-exchange was the level of deuterium present in the buffer (64.32%). Changes in any peptide at any time point greater than 5% and 0.5 Da between conditions with a unpaired t test value of $p < 0.01$ were considered significant. Full deuterium incorporation data for all analyzed peptides are included in Table S1.

Rab5–PI3Kβ kinase assay

Expression constructs (p85α-FLAG(×3) and p110β-StrepII(×3)) were transfected into a 30-ml culture of Expi293F cells (Gibco) following the manufacturer's protocol. 72 h post-transfection, the cells were harvested by centrifugation and resuspended in 2 ml of lysis buffer (20 mM Tris-HCl, pH 7.4, 150 mM NaCl, 1% Tween 20, 1 mM DTT, 1 mM $MgCl_2$, 10% glycerol, protease inhibitor mixture (cOmplete, EDTA-free, Roche Applied Science)). Cells were lysed by rotating at 4 °C for 15 min and cleared by centrifugation at 13,000 × g for 10 min. The soluble lysate was incubated with a 100-μl slurry of Strep-Tactin Superflow high-capacity beads (IBA Lifesciences) for 60 min at 4 °C with rotation. Beads were washed three times in wash buffer (20 mM Tris-HCl, pH 7.4, 150 mM NaCl, 1 mM DTT, 1 mM $MgCl_2$, 10% glycerol, protease inhibitors). Protein was eluted in two sequential fractions of 100 μl in elution buffer (wash buffer with addition of 5 mM desthiobiotin). The eluted proteins were pooled and dialyzed overnight against kinase assay buffer (as described above). Purity was assessed by SDS-PAGE, and protein concentration was determined by absorbance. Aliquots were flash frozen and stored at −80 °C in assay buffer.

Recombinant GST-Rab5 was produced as described above, immobilized on GSH-agarose, and cleaved by overnight incubation with recombinant tobacco etch virus protease at 4 °C. The cleaved Rab5 was eluted and dialyzed into kinase assay buffer. Protein purity was determined by SDS-PAGE, and protein concentration was determined by absorbance. Nucleotide loading was achieved by incubation of Rab5 with 1 mM EDTA and 10 mM nucleotide (GDP or GTPγS) for 20 min at 30 °C followed by the addition of $MgCl_2$ (3 mM final in Rab5 mixture). The protein was incubated for an additional 3 min at 30 °C and then stored on ice.

Lipid vesicles (dioleophosphatidylcholine:dioleophosphatidylserine:cholesterol:bovine brain PIP_2 at 30.1:47.6:10.3:2.9 mol %) were dried under nitrogen, lyophilized overnight, and resuspended by vortexing in 20 mM PIPES, pH 6.5, 100 mM NaCl, 2 mM EGTA, 0.1% (w/v) CHAPS at a final lipid concentration of 2 mM. Liposomes were prepared by 30 passes through an Avanti extruder (pore size, 100 μm). Vesicle size (usually ~60–75-nm radius) was analyzed by dynamic light scattering (Dynapro, Wyatt Technologies).

Recombinant PI3Kβ (17.6 nM final) was incubated with freshly prepared vesicles (37 μM PIP_2 final) and GDP- or GTP-loaded Rab5 (10 μM final) or bistyrosyl phosphopeptide (DDG-pYMPMSPGAGAGAGAGAGNEDpYMPMSPKS; 1 μM) for 10 min. Assays were started by the addition of ATP (100 μM final) containing 10 μCi of [^{32}P]ATP. 4-μl aliquots were spotted onto nitrocellulose filters every 2 min. Filters were washed, and radioactivity was quantitated as described above. Activity is expressed as the slope of the progress curve between 0 and 10 min as determined by nonlinear regression.

Cell-based assays

Stable MDA-MBA231 p110β knockdown/rescue cell lines expressing WT and kinase-dead p110β have been described previously (20). Knockdown/rescue cells expressing Rab5-uncoupled p110β were produced using the same methods. Transwell migration and invasion assays using MDA-MB-231 cells stably expressing WT or mutant p110β have been described previously (20). For the chemotaxis assay, breast cancer cells were serum-starved overnight and seeded in starvation medium in the upper chamber of transwell inserts coated with 10 μg/ml fibronectin (Sigma). The lower chambers contained starvation medium without or with 10 μM LPA or 5 nM EGF (EMD Millipore). Cells were allowed to chemotax for 8 h at 37 °C. For the invasion assay, serum-starved cells were seeded onto transwell inserts coated with 300 μg/ml growth factor–reduced Matrigel (BD Biosciences). The lower chambers contained starvation medium without or with 5 nM EGF. Cells were allowed to invade for 24 h.

Degradation of Oregon Green 488–conjugated gelatin (Molecular Probes) by MDA-MB-231 cells stably expressing WT or mutant PI3Kβ has been described previously (20). Cells were imaged, and the area of matrix degradation per cell was quantitated using ImageJ software.

Statistical analysis

Statistical analyses were performed using GraphPad Prism version 7.0c (GraphPad Software) to calculate the p values for one-way ANOVA and unpaired Student's t tests.

Author contributions—S. D. H., D. J. H., R. M. H., N. G., G. S., Z. E., J. E. B., J. U. F., A. R. B., and J. M. B. formal analysis; S. D. H., D. J. H., R. M. H., N. G., G. S., Z. E., B. D. K., J. E. B., J. U. F., A. R. B., and J. M. B. investigation; S. D. H., D. J. H., R. M. H., G. S., B. D. K., A. S., E. A. S., and G. Q. G. methodology; S. D. H. writing-original draft; S. D. H., J. E. B., A. R. B., and J. M. B. writing-review and editing; B. D. K., A. S., and B. N. resources; G. Q. G., J. E. B., J. U. F., A. R. B., and J. M. B. conceptualization; J. E. B., J. U. F., A. R. B., and J. M. B. supervision; A. R. B. and J. M. B. funding acquisition; A. R. B. and J. M. B. project administration.

References

1. Vanhaesebroeck, B., Leevers, S. J., Ahmadi, K., Timms, J., Katso, R., Driscoll, P. C., Woscholski, R., Parker, P. J., and Waterfield, M. D. (2001)

Synthesis and function of 3-phosphorylated inositol lipids. *Annu. Rev. Biochem.* **70,** 535–602 CrossRef Medline
2. Vanhaesebroeck, B., Guillermet-Guibert, J., Graupera, M., and Bilanges, B. (2010) The emerging mechanisms of isoform-specific PI3K signalling. *Nat. Rev. Mol. Cell Biol.* **11,** 329–341 CrossRef Medline
3. Zhang, X., Vadas, O., Perisic, O., Anderson, K. E., Clark, J., Hawkins, P. T., Stephens, L. R., and Williams, R. L. (2011) Structure of lipid kinase p110β/p85β elucidates an unusual SH2-domain-mediated inhibitory mechanism. *Mol. Cell* **41,** 567–578 CrossRef Medline
4. Kurosu, H., Maehama, T., Okada, T., Yamamoto, T., Hoshino, S., Fukui, Y., Ui, M., Hazeki, O., and Katada, T. (1997) Heterodimeric phosphoinositide 3-kinase consisting of p85 and p110β is synergistically activated by the βγ subunits of G proteins and phosphotyrosyl peptide. *J. Biol. Chem.* **272,** 24252–24256 CrossRef Medline
5. Dbouk H. A., Vadas, O., Shymanets, A., Burke, J. E., Salamon, R. S., Khalil, B. D., Barrett, M. O., Waldo, G. L., Surve, C., Hsueh, C., Perisic, O., Harteneck, C., Shepherd, P. R., Harden, T. K., Smrcka, A. V., *et al.* (2012) G protein-coupled receptor-mediated activation of p110β by Gβγ is required for cellular transformation and invasiveness. *Sci. Signal.* **5,** ra89 CrossRef Medline
6. Fritsch, R., de Krijger, I., Fritsch, K., George, R., Reason, B., Kumar, M. S., Diefenbacher, M., Stamp, G., and Downward, J. (2013) RAS and RHO families of GTPases directly regulate distinct phosphoinositide 3-kinase isoforms. *Cell* **153,** 1050–1063 CrossRef Medline
7. Christoforidis, S., Miaczynska, M., Ashman, K., Wilm, M., Zhao, L., Yip, S. C., Waterfield, M. D., Backer, J. M., and Zerial, M. (1999) Phosphatidylinositol-3-OH kinases are Rab5 effectors. *Nat. Cell Biol.* **1,** 249–252 CrossRef Medline
8. Chiariello, M., Bruni, C. B., and Bucci, C. (1999) The small GTPases Rab5a, Rab5b and Rab5c are differentially phosphorylated *in vitro*. *FEBS Lett.* **453,** 20–24 CrossRef Medline
9. Langemeyer, L., Nunes Bastos, R., Cai, Y., Itzen, A., Reinisch, K. M., and Barr, F. A. (2014) Diversity and plasticity in Rab GTPase nucleotide release mechanism has consequences for Rab activation and inactivation. *Elife* **3,** e01623 CrossRef Medline
10. Ciraolo, E., Iezzi, M., Marone, R., Marengo, S., Curcio, C., Costa, C., Azzolino, O., Gonella, C., Rubinetto, C., Wu, H., Dastrù, W., Martin, E. L., Silengo, L., Altruda, F., Turco, E., *et al.* (2008) Phosphoinositide 3-kinase p110β activity: key role in metabolism and mammary gland cancer but not development. *Scie. Signal.* **1,** ra3 CrossRef Medline
11. Jia, S., Liu, Z., Zhang, S., Liu, P., Zhang, L., Lee, S. H., Zhang, J., Signoretti, S., Loda, M., Roberts, T. M., and Zhao, J. J. (2008) Essential roles of PI(3)K-p110β in cell growth, metabolism and tumorigenesis. *Nature* **454,** 776–779 CrossRef Medline
12. Dou, Z., Pan, J. A., Dbouk, H. A., Ballou, L. M., DeLeon, J. L., Fan, Y., Chen, J. S., Liang, Z., Li, G., Backer, J. M., Lin, R. Z., and Zong, W. X. (2013) Class IA PI3K p110β subunit promotes autophagy through Rab5 small GTPase in response to growth factor limitation. *Mol. Cell* **50,** 29–42 CrossRef Medline
13. Salamon, R. S., Dbouk, H. A., Collado, D., Lopiccolo, J., Bresnick, A. R., and Backer, J. M. (2015) Identification of the Rab5 binding site in p110β: assays for PI3Kβ binding to Rab5. *Methods Mol. Biol.* **1298,** 271–281 CrossRef Medline
14. Chamberlain, M. D., Berry, T. R., Pastor, M. C., and Anderson, D. H. (2004) The p85α subunit of phosphatidylinositol 3′-kinase binds to and stimulates the GTPase activity of Rab proteins. *J. Biol. Chem.* **279,** 48607–48614 CrossRef Medline
15. Whitecross, D. E., and Anderson, D. H. (2017) Identification of the binding sites on Rab5 and p110β phosphatidylinositol 3-kinase. *Sci. Rep.* **7,** 16194–16194 CrossRef Medline
16. Chen, P. I., Kong, C., Su, X., and Stahl, P. D. (2009) Rab5 isoforms differentially regulate the trafficking and degradation of epidermal growth factor receptors. *J. Biol. Chem.* **284,** 30328–30338 CrossRef Medline
17. Chen, P. I., Schauer, K., Kong, C., Harding, A. R., Goud, B., and Stahl, P. D. (2014) Rab5 isoforms orchestrate a "division of labor" in the endocytic network; Rab5C modulates Rac-mediated cell motility. *PLoS One* **9,** e90384 CrossRef Medline
18. Zheng, Y., Bagrodia, S., and Cerione, R. A. (1994) Activation of phosphoinositide 3-kinase activity by Cdc42Hs binding to p85. *J. Biol. Chem.* **269,** 18727–18730 Medline
19. Tolias, K. F., Cantley, L. C., and Carpenter, C. L. (1995) Rho family GTPases bind to phosphoinositide kinases. *J. Biol. Chem.* **270,** 17656–17659 Medline
20. Khalil, B. D., Hsueh, C., Cao, Y., Abi Saab, W. F., Wang, Y., Condeelis, J. S., Bresnick, A. R., and Backer, J. M. (2016) GPCR signaling mediates tumor metastasis via PI3Kβ. *Cancer Res.* **76,** 2944–2953 CrossRef Medline
21. Dbouk, H. A., Pang, H., Fiser, A., and Backer, J. M. (2010) A biochemical mechanism for the oncogenic potential of the p110β catalytic subunit of phosphoinositide 3-kinase. *Proc. Natl. Acad. Sci. U.S.A.* **107,** 19897–19902 CrossRef Medline
22. Mandelker, D., Gabelli, S. B., Schmidt-Kittler, O., Zhu, J., Cheong, I., Huang, C.-H., Kinzler, K. W., Vogelstein, B., and Amzel, L. M. (2009) A frequent kinase domain mutation that changes the interaction between PI3Kα and the membrane. *Proc. Natl. Acad. Sci. U.S.A.* **106,** 16996–17001 CrossRef Medline
23. Hanahan, D., and Weinberg, R. A. (2011) Hallmarks of cancer: the next generation. *Cell* **144,** 646–674 CrossRef Medline
24. Frittoli, E., Palamidessi, A., Marighetti, P., Confalonieri, S., Bianchi, F., Malinverno, C., Mazzarol, G., Viale, G., Martin-Padura, I., Garré, M., Parazzoli, D., Mattei, V., Cortellino, S., Bertalot, G., Di Fiore, P. P., *et al.* (2014) A RAB5/RAB4 recycling circuitry induces a proteolytic invasive program and promotes tumor dissemination. *J. Cell Biol.* **206,** 307–328 CrossRef Medline
25. Yuzugullu, H., Baitsch, L., Von, T., Steiner, A., Tong, H., Ni, J., Clayton, L. K., Bronson, R., Roberts, T. M., Gritsman, K., and Zhao, J. J. (2015) A PI3K p110β–Rac signalling loop mediates Pten-loss-induced perturbation of haematopoiesis and leukaemogenesis. *Nat. Commun.* **6,** 8501 CrossRef Medline
26. Deleted in proof
27. Huang, C. H., Mandelker, D., Schmidt-Kittler, O., Samuels, Y., Velculescu, V. E., Kinzler, K. W., Vogelstein, B., Gabelli, S. B., and Amzel, L. M. (2007) The structure of a human p110α/p85α complex elucidates the effects of oncogenic PI3Kα mutations. *Science* **318,** 1744–1748 CrossRef Medline
28. Dornan, G. L., Siempelkamp, B. D., Jenkins, M. L., Vadas, O., Lucas, C. L., and Burke, J. E. (2017) Conformational disruption of PI3Kδ regulation by immunodeficiency mutations in PIK3CD and PIK3R1. *Proc. Natl. Acad. Sci. U.S.A.* **114,** 1982–1987 CrossRef Medline
29. Wu, H., Shekar, S. C., Flinn, R. J., El-Sibai, M., Jaiswal, B. S., Sen, K. I., Janakiraman, V., Seshagiri, S., Gerfen, G. J., Girvin, M. E., and Backer, J. M. (2009) Regulation of Class IA PI 3-kinases: C2 domain-iSH2 domain contacts inhibit p85/p110α and are disrupted in oncogenic p85 mutants. *Proc. Natl. Acad. Sci. U.S.A.* **106,** 20258–20263 CrossRef Medline
30. Jimenez, C, Jones, D. R., Rodríguez-Viciana, P., Gonzalez-García, A., Leonardo, E., Wennström, S., von Kobbe, C., Toran, J. L., R-Borlado, L., Calvo, V., Copin, S. G., Albar, J. P., Gaspar, M. L., Diez, E., Marcos, M. A., *et al.* (1998) Identification and characterization of a new oncogene derived from the regulatory subunit of phosphoinositide 3-kinase. *EMBO J.* **17,** 743–753 CrossRef Medline
31. Jaiswal, B. S., Janakiraman, V., Kljavin, N. M., Chaudhuri, S., Stern, H. M., Wang, W., Kan, Z., Dbouk, H. A., Peters, B. A., Waring, P., Dela Vega, T., Kenski, D. M., Bowman, K. K., Lorenzo, M., Li, H., *et al.* (2009) Somatic mutations in p85α promote tumorigenesis through class IA PI3K activation. *Cancer Cell* **16,** 463–474 CrossRef Medline
32. Studier, F. W. (2005) Protein production by auto-induction in high-density shaking cultures. *Protein Expr. Purif.* **41,** 207–234 CrossRef Medline
33. Shymanets, A., Prajwal, Vadas, O., Czupalla, C., LoPiccolo, J., Brenowitz, M., Ghigo, A., Hirsch, E., Krause, E., Wetzker, R., Williams, R. L., Harteneck, C., and Nürnberg, B. (2015) Different inhibition of Gβγ-stimulated class IB phosphoinositide 3-kinase (PI3K) variants by a monoclonal antibody. Specific function of p101 as a Gβγ-dependent regulator of PI3Kγ enzymatic activity. *Biochem. J.* **469,** 59–69 CrossRef Medline
34. Longo, P. A., Kavran, J. M., Kim, M. S., and Leahy, D. J. (2013) Transient mammalian cell transfection with polyethylenimine (PEI). *Methods Enzymol.* **529,** 227–240 CrossRef Medline
35. Knight, Z. A., Feldman, M. E., Balla, A., Balla, T., and Shokat, K. M. (2007) A membrane capture assay for lipid kinase activity. *Nat. Protoc.* **2,** 2459–2466 CrossRef Medline